JB BIOCHEMISTRY

Inhibition study on insulin fibrillation and cytotoxicity by paclitaxel

Received January 13, 2014; accepted January 28, 2014; published online February 17, 2014

Ehsan Kachooei[1,a], Ali Akbar Moosavi-Movahedi[1,2,*], Fariba Khodagholi[3], Faroogh Mozaffarian[1,a], Payam Sadeghi[3,a], Hamid Hadi-Alijanvand[4], Atiyeh Ghasemi[1], Ali Akbar Saboury[1,2], Mohammad Farhadi[5] and Nader Sheibani[6]

[1]Institute of Biochemistry and Biophysics, University of Tehran, Tehran, Iran; [2]Center of Excellence in Biothermodynamics, University of Tehran, Tehran, Iran; [3]NeuroBiology Research Center, Shahid Beheshti University of Medical Sciences, Tehran, Iran; [4]Department of Biological Sciences, Institute for Advanced Studies in Basic Sciences, Department of Biological Sciences, Zanjan, Iran; [5]ENT-HNS Research Center, IUMS, Tehran, Iran; and [6]Department of Ophthalmology and Visual Sciences, University of Wisconsin School of Medicine and Public Health, Madison, WI 53792, USA; [a]These authors contributed to this work equally

*Ali Akbar Moosavi-Movahedi, Institute of Biochemistry and Biophysics, University of Tehran, Tehran, Iran.
Tel: +9821-66403957, Fax: +9821-66404680,
email: moosavi@ut.ac.ir

Alzheimer, a neurodegenerative disease, and a large variety of pathologic conditions are associated with a form of protein aggregation known as amyloid fibrils. Since fibrils and prefibrillar intermediates are cytotoxic, numerous attempts have been made to inhibit fibrillation process as a therapeutic strategy. Peptides, surfactants and aromatic small molecules have been used as fibrillation inhibitors. Here we studied the effects of paclitaxel, a polyphenol with a high tendency for interaction with proteins, on fibrillation of insulin as a model protein. The effects of paclitaxel on insulin fibrillation were determined by Thioflavin T fluorescence, Congo red absorbance, circular dichroism and atomic force microscopy. These studies indicated that paclitaxel considerably hindered nucleation, and therefore, fibrillation of insulin in a dose-dependant manner. The isothermal titration calorimetry studies showed that the interaction between paclitaxel and insulin was spontaneous. In addition, the van der Waal's interactions and hydrogen bonds were prominent forces contributing to this interaction. Computational results using molecular dynamic simulations and docking studies revealed that paclitaxel diminished the polarity of insulin dimer and electrostatic interactions by increasing the hydrophobicity of its dimer state. Furthermore, paclitaxel reduced disrupting effects of insulin fibrils on PC12 cell's neurite outgrowth and complexity, and enhanced their survival.

Keywords: cytotoxicity/inhibition/insulin fibrillation/nucleation/paclitaxel.

Abbreviations: AFM, atomic force microscope; DMEM, Dulbecco's modified Eagle's medium; ITC, isothermal titration calorimetry; MTT, 3-[4, 5-dimethylthiazol-2-yl]-2,5-diphenyl tetrazolium bromide; ThT, Thioflavin T.

It is a natural tendency of proteins to be misfolded with disruption of their native conformation. Among misfolded proteins a group of similar structural deposits named amyloid fibrils tend to aggregate with some particular traits, either systemically or locally in certain organs or tissues, and cause amyloidosis (*1*, *2*). Long and un-branched filaments sharing a cross-β structure are particularly attributed to fibril components of amyloid diseases (*1–5*). Alzheimer's disease, type II diabetes, insulin-related amyloidosis, lysozyme amyloidosis and the majority of the amyloid diseases are evidently associated with debilitating conditions and aging (*2*). Recently, development of *in vitro* model systems to study amyloid formation, and its detailed structural, kinetic and thermodynamic characteristics has become widely possible. In the case of globular proteins, amyloid forms are produced under denaturing conditions (*6*, *7*).

The toxicity of amyloid aggregates is an inherent characteristic, which is correlated with common structural backbone and not with specific tracks of residues (*8*). Thus, many efforts are being made to find suitable solutions to inhibit fibril formation. Surfactants (*9*), peptides (*10*), small molecules (*11*, *12*), nanoparticles (*13*), polyphenols (*14–16*) and even glycation (*17*) are considered for their possible inhibitory effects. Among these, the natural and synthetic polyphenols have shown a great tendency to inhibit amyloid fibril formation (*14*). The Polyphenol's inhibitory effects have been observed with different amyloidogenic proteins *in vitro*, in cell culture and *in vivo* (*16*, *18*).

Paclitaxel (Taxol®) is a complex diterpene isolated from Taxus brevifolia. Due to its ability to bind and stabilize the cytoplasmic microtubules (*19–21*), and thus block the cell cycle in G_2 and M phase, paclitaxel has become an important antimitotic and antitumour agent (*22*). It has been also reported that there is a functional taxoid-binding site on tubulin dimers (*23*, *24*). Paclitaxel is also clinically used for the treatment of refractory ovarian cancer and many other tumour types including lung, breast, prostate, and head and neck cancer (*25*). Microtubule stabilizing agents have also been suggested for use against Alzheimer-type neuropathogenesis, since they could protect neurons against β-amyloid toxicity (*26*). Aromatic rings in the structure of paclitaxel suggest that paclitaxel may

inhibit amyloid formation through the effects of its aromatic interactions.

Insulin is a small globular protein with a molecular weight of approximately 5,783 Da, and is consist of two helical chains linked together by two disulfide bonds (*27*, *28*). In the laboratory and under conditions like high temperature, high concentration and low pH which cause partially unfolded intermediates, insulin molecules undergo the process of fibrillation (*29–32*). In some studies, insulin fibrillar forms and prefibrillar intermediates have shown cytotoxicity on rat pheochromocytoma PC12 (*9*, *33*) and pancreatic β-cells (*34*). It seems that insulin fibrillation initiates with the partial unfolding of the monomers, followed by further association into protein oligomers, and finally formation of mature amyloid aggregates (*30*, *35*). Bovine insulin is one of the best-characterized proteins, and used in many studies including assessment of its three-dimensional structure, folding–unfolding mechanisms, unfolding intermediates and stability information (*36*). Thus, insulin is a suitable model to explore protein fibrillation.

In the present study, we explored insulin fibrillation under acidic pH and high temperature, and determined the effects of paclitaxel on this process. Moreover, in order to deliberate how and by what mechanisms paclitaxel interacts with insulin, isothermal calorimetry and docking simulation were performed. In our previous study, we explored the surface properties of fibrillar insulin and its intermediates, and found the association of this characteristic with cytotoxicity because of detergent-like effect of them, especially for oligomeric forms. The aim of this work was to study the interaction of paclitaxel, as a polyphenol small molecule, with insulin and its high potency for inhibition of insulin amyloid fibrillation. This criterion was considered based on paclitaxel high tendency to interact with proteins. Here, the fibrillar form of insulin has just been studied. Finally, the impact of insulin fibrils incubated with paclitaxel on neuronal-like PC12 cell differentiation was investigated by considering neurite outgrowth and complexity criteria, cell viability and apoptosis, as a complementary study to better illustrate the modulating effect of paclitaxel on insulin amyloid fibrillation and cytotoxicity.

Experimental Procedures

Chemical

Bovine pancreas insulin (code I5500), ThT, Congo red, MTT (3-[4, 5-dimethylthiazol-2-yl]-2,5-diphenyl tetrazolium bromide), nerve growth factor (NGF) and Dulbecco's modified Eagle's medium (DMEM) were purchased from Sigma-Aldrich (St. Louis, MO, USA). Horse serum and fetal bovine serum were obtained from Life Technologies (Carlsbad, CA, USA). Paclitaxel (taxol) purchased from Stragen (Switzerland). Sodium phosphate was from Merck (Germany).

Sample preparation

Insulin powder was dissolved in aqueous HCl solution (pH 2.0) and insulin concentration was determined by measuring absorbance at 276 nm with excitation coefficients of 1 mg/ml using an UV-3100 Shimadzu UV-Vis-NIR spectrophotometer (Japan). The pH of the solution was adjusted to 1.6 prior to incubation. Fibrils were prepared by incubating insulin solution (500 μM) at 57°C. For inhibition studies, paclitaxel was diluted with aqueous HCl solution (pH 2.0) and added to insulin solution in amounts that kept insulin concentration constant with ratios of 1:1000, 1:100 and 1:10 (paclitaxel:insulin; P:I).

Congo red absorbance

The Congo red solution (20 μM) was prepared by dissolving Congo red powder in 25 mM sodium phosphate buffer (pH 6.0). Following incubation, 24 μl of each sample (insulin was diluted 6-fold) was mixed with 176 μl of Congo red and incubated for 10 min at room temperature in the dark. Using a quartz cell with 1 cm path length and a UV-Vis-NIR spectrophotometer (model UV-3100, Shimadzu, Japan), absorbance spectrum of each protein sample was recorded from 400 to 700 nm. Each spectrum is the average of three independent measurements.

ThT assay

Thioflavin T (ThT) assay is a useful fluorometric method for determination of amyloid fibrils *in vitro* (*37*). ThT was dissolved in 25 mM sodium phosphate buffer (pH 6.0) by vortexing and passed through a 0.4 μm filter. ThT concentration was determined by measuring absorbance at 416 nm with a molar extinction coefficient of 26,600 $M^{-1}\,cm^{-1}$(*10*). At different time intervals, an aliquot (10 μl for insulin) was diluted with ThT solution (20 μM) to 500 μl. Fluorescence measurements were conducted using Cary Eclipse fluorescence spectrophotometer (Varian, Australia) in a quartz cuvette with 1 cm path length. The excitation and emission wavelengths were adjusted at 440 nm and 485 nm, respectively, with 5 nm slit width for both. According to Nielsen *et al.* study (*38*), the acquired data from ThT fluorescence measurements were fitted to the sigmoid curve represented by the pursuant equation:

$$F = F_{\min} + \frac{F_{\max}}{1 + e^{-[(t-t_0)/\tau]}},$$

whereas F is fluorescence intensity, the incubation time is t and t_0 is the time to obtain 50% of maximal fluorescence. Thus, using the acquired value of τ by nonlinear regression, the apparent growth rate constant of fibrils and lag phase were defined by $1/\tau$ and $t_0 - 2\tau$, respectively. Each point is the average of three independent measurements.

Circular dichroism spectroscopy

Secondary structure analysing was done using Far-UV-CD. Insulin samples were diluted 6-fold with aqueous HCl (pH 2.0) in a quartz cell with a 1 mm path length. Using a spectropolarimeter (model J-810, Jasco, Japan) the CD spectra was recorded by scanning the sample from 195 to 260 nm at the ambient temperature. Bandwidth of 1 nm, slit width of 0.02 mm and speed of 50 $nm\,s^{-1}$ was considered for each scanning. Each spectrum is the average of five scan and CD spectra of aqueous HCl was subtracted from insulin spectra.

Atomic force microscopy

Fibrillar structure of insulin was visualized using atomic force microscopy. An aliquot (10 μl) of incubated solution was diluted 300-fold in aqueous HCl (pH 2.0) and 10 μl of diluted sample was placed on lamella (freshly washed with distilled water and alcohol) and dried at room temperature. Images were acquired in non-contact mode with a loop filter of 2 Hz and force of 5.5–22.5 N/m. Each scan was done in a $5 \times 5\,\mu m^2$ area, using an AFM (Autoprobe CP research, Veeco, USA) and conical shape silicon tip with resonance frequency of 190–325 kHz. The analysis of images was performed using 'ProScan 1.7' software. For determining diameter and height of particles 10 particles in each image were selected randomly, then the average and standard deviation were calculated.

Isothermal titration calorimetry

In order to explore the interaction of paclitaxel with insulin, isothermal titration calorimetry (ITC) technique was used with a VP-ITC (Microcal, USA). All solutions (buffer, insulin and paclitaxel) were degassed at 25°C while stirring, before experiment. Stirring of insulin was done in low rate and paclitaxel was done in high rate for 3 min using thermovac (sample degassing and thermostat). The sample and reference cell were filled with 1.8 ml of insulin (15 μM) and 1.8 ml of buffer (aqueous HCl, pH 1.6), respectively. Each cell was coin shaped and adiabatic. The syringe was filled with 300 μl of paclitaxel

(150 μM) which was injected into the sample cell in 30 steps. In the first step 5 μl of paclitaxel in the period of 10 s, and the other steps 10 μl in the period of 20 s were injected. The heat exchange was recorded using Microcal ORIGIN software (v.7.0), once for interaction of paclitaxel with insulin and once for dilution of insulin. Then dilution heat was subtracted from interaction heat, the acquired curves were fitted in *one set of site* model, and thermodynamic parameters including number of sites (N), affinity constant (K), enthalpy (ΔH) and entropy (ΔS) changes were obtained by frequent curve fitting of binding isotherms using Origin 7. The Gibbs free energy (ΔG) change was calculated from following equation ($\Delta G = \Delta H - T\Delta S$).

Computational approaches

The 3D structure of paclitaxel and insulin are refined by short MD after energy minimization in aqueous condition. The docking computation was performed by HEX 6. The best results (based on binding energy) of docking output was analysed in VMD software. Swiss PDB viewer program was utilized to compute electrostatic potential of molecules.

Cell culture and PC12 cells differentiation

Rat pheochromocytoma (PC12) cells were obtained from Pasteur Institute (Tehran, Iran). The cells were grown in DMEM containing 5% fetal bovine serum, 10% horse serum, and 1% penicillin–streptomycin at 37°C and 5% CO_2. To induce differentiation, PC12 cells were incubated with NGF (50 ng/ml) every other day for 6 days. Growth medium was changed three times a week.

Treatment conditions and morphological determination of PC12 cells

Differentiated PC12 cells, seeded in 6-well plates, were pre-incubated with paclitaxel (50 μM) 2 h prior to initiation of the experiments. The cells were then incubated with 25 μM of insulin fibrils (incubated for 420 min, with concentration of 500 μM; prepared in the absence or the presence of different concentrations of paclitaxel 0.5, 5 and 50 μM) for 2, 5, 8 and 12 h. For morphological analysis, two random images were acquired from each well by phase contrast microscopy (Olympus IX71, Japan). A minimum of 50 cells per treatment were quantified. The cell body was the criteria for selection. The cell processes were completely within the field of view, and the body of an individual cell was distinct from neighbouring cells. Cells fitting these criteria were analysed and their cell body area, average neurite length, neurite width, and the number of primary neurites and bipolar morphology were quantified.

Cell body area was defined as the area of the cell that neurite processes originate from and contained cell organelles. Neurite length was calculated by summing the lengths of the primary processes and all associated branches. To establish the average neurite width, the outlines of individual primary neurites were traced. The cell body area was calculated by Cell A software and then divided by the length of the neurites. Primary neurites were defined as clear protrusions from the cell body that are greater than 10 μm in length. Cells were considered 'bipolar' if they displayed a cell body with one process at each end. To evaluate neurite networks, images were analysed using the cell counter plug-in to score all branching nodes in each image. Nodes were defined as sites where individual neurites branched or separate neurites contacted each other. All measurements were expressed as proportions of cells displaying the characteristics of a sub-population of the total number of cells which met the selection criteria described above. A sample of this processing is shown in Fig. 7A.

Measurement of cell viability employing MTT assay and Hoechst staining

Conventional MTT reduction assay was utilized to determine cell viability. The live cells turned dark blue because of formation of formazan crystals from mitochondrial oxidation. Dimethyl sulfoxide (DMSO) was used to solubilize the coloured crystals and the absorbance was measured at 550 nm. The percentage of cell viability was determined as the percentage of reduced MTT, considering the absorbance of control cells as 100%.

Hoechst 33342 (Invitrogen, H3570) staining as a criteria for detection of apoptotic cells was also conducted. Differentiated PC12 cells were cultured in a 96-well plate and were incubated with insulin fibrils prepared without or with 50 μM paclitaxel for different times. Cells were harvested at appropriate times and washed three times with phosphate buffer saline. The cells were then incubated for 5 min at room temperature with Hoechst 33342 (1 μg/ml) and nuclei were visualized using fluorescence microscopy (Olympus).

Statistical analysis

All experiments were conducted at least three times and the final data are represented as the mean ± S.E.M. Comparison between groups was made by one-way analysis of variance (ANOVA) followed by a specific *post hoc* test to analyse the difference. Mean differences were considered significant when $p<0.05$ (*or $^{\#}p<0.05$, **or $^{\#\#}p<0.01$ and ***p or $^{\#\#\#}p<0.001$).

Results

Paclitaxel reduces formation of beta-sheet structures and delays nucleation of insulin

Congo red and ThT are markers for recognition of beta-sheet structures (*39*). Fig. 1A shows no considerable differences, before incubation, between the Congo red spectra of insulin alone or with different concentrations of paclitaxel compared to Congo red spectrum. Following incubation, a significant increase in Congo red absorbance and a red shift to 540 nm was observed for insulin compared with the native form. However, in the presence of paclitaxel the trends of Congo red absorbance were very different. At lower concentration of paclitaxel (0.5 μM with a ratio of 1:1000, P:I), absorbance intensity and red shift decreased a little, but at higher concentration of paclitaxel (50 μM with ratio of 1:10, P:I) absorbance spectrum intensity of Congo red was significantly decreased and the red shift diminished compared with control. Thus, the Congo red spectrum of insulin in the presence of paclitaxel was similar to the native form.

The kinetic of fibrillation was acquired using ThT fluorescence emission at 485 nm. These results showed that fibrillation of insulin had a three state sigmoid profile including: a lag phase, elongation phase and saturation phase. Fig. 1B shows the trends of insulin fibrillation in the presence and absence of paclitaxel. In low concentration of paclitaxel with ratio 1:1000 (P: I), an increase in lag phase was observable in insulin fibrillation. However, with an increase in elongation rate, fibrillation process reached a plateau. There was no significant change in saturation phase intensity of insulin fibrillation. With increased paclitaxel concentration, the lag phase increased directly, and the saturation phase occurred to a lower extent compared to control indicating that the formation of fibrils was reduced.

The extent of alterations in the lag phase and maximum fibrillation was most evident when insulin was pre-incubated with 50 μM of paclitaxel. Alterations in the kinetic parameters including lag phase and growth rate of fibrillation were affected by various concentrations of paclitaxel and are summarized in Table I. With increased paclitaxel concentration up to 50 μM, the lag phase and growth rate of fibrillation were increased, and the ratio of fibril formation was decreased to 38%.

In order to explore the efficacy of paclitaxel on elongation phase, 20 μM of fibrils which it had been prepared already, were added to insulin solutions (without and with paclitaxel) before incubation. As it

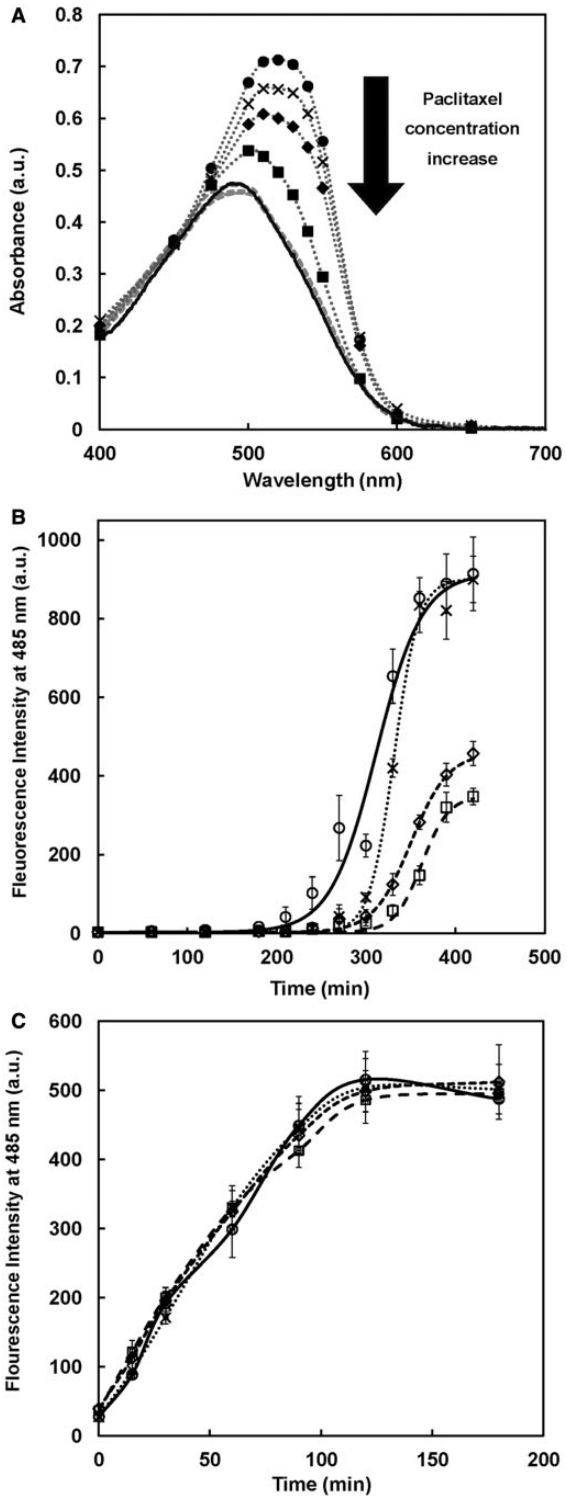

Fig. 1 Paclitaxel reduced insulin fibrillation and delayed nucleation. (**A**) Congo red absorption of insulin indicating the content of fibril formation before incubation (dashed lines) and after incubation (dotted lines) with various concentrations of paclitaxel: 0 (filled circle), 0.5 (times), 5 (filled diamond) and 50 (filled square) μM at pH 1.6 and 57°C. Absorbance of Congo red alone is shown by the solid line. (**B**) The kinetic of insulin fibrillation recorded via ThT fluorescence emission at 485 nm with different concentration of paclitaxel: 0 (open circle), 0.5 (times), 5 (open diamond) and 50 (open square) μM. (**C**) The elongation phase of insulin fibrillation recorded via ThT fluorescence by conditions which mentioned in previous part. Each emission point is the average of three independent measurements, and error bars represent standard deviation from the mean value.

was shown in Fig. 1C, fibrillation is commenced at the onset of incubation and presence of paclitaxel in different concentrations (0.5, 5 and 50 μM) did not impress the process of insulin fibrillation. This study indicates that paclitaxel did not affect on elongation phase of insulin fibrillation.

Stabilization of insulin secondary structure in the presence of paclitaxel

Secondary structure analysis of insulin with circular dichroism before incubation showed two minima around 208 and 222 nm, which indicated the dominant alpha secondary structure of insulin (*29*). In addition, the presence of different concentrations of paclitaxel in insulin solutions did not result in secondary structure changes (Fig. 2A). Following incubation, the former minima were vanished, and another minimum appeared around 216 nm, which is a characteristic of beta-sheet secondary structure. In the presence of increasing concentration of paclitaxel significant differences were observed in the insulin secondary structure. In 0.5 μM paclitaxel (with ratio of 1:1000, P:I), the secondary structure of insulin did not change significantly compared with no paclitaxel. Samples which were incubated with 5 μM and 50 μM paclitaxel (ratios of 1:100 and 1:10, P:I) showed a dramatic change in CD spectra, and the spectrum minimum shifted to near 208 nm (Fig. 2B). These results indicated that in the presence of higher concentrations of paclitaxel the secondary structure of insulin remained near the native form, and little monomers converted to fibrils.

Paclitaxel inhibited the growth and lateral aggregation of mature insulin amyloid fibrils

In order to visualize morphological characteristics of fibrils AFM images from each sample was acquired following incubation with or without paclitaxel. Under experimental conditions (acidic pH and 57°C) monomers of insulin converted to fibrillar insulin. Fig. 3A shows that the insulin fibrils were prominent. In the presence of paclitaxel (50 μM) the insulin fibrils were less prominent and became partially shorter and thinner compared to no paclitaxcel (Fig. 3A). The three micrometer scale image of each sample annexation with diameter graph of fibrils is depicted in Fig. 3B. The diameter of insulin fibrils which prepared without and with paclitaxel was 104.38 ± 3.34 nm and 57.53 ± 5.21 nm, respectively. Also the height of fibrils on the surface of lamella was 9.16 ± 0.86 nm and 5.71 ± 0.57 nm in the absence and presence of paclitaxel, respectively. As depicted in the image, following incubation of insulin with paclitaxel the diameter and height of the fibrils became smaller compared to fibrils formed in the absence of paclitaxel. Furthermore, spherical shapes were observed in AFM images in the presence of paclitaxel and imply oligomer formation (Fig. 3C). The diameter and height of oligomers were obtained 34.87 ± 2.06 nm and 1.75 ± 0.11 nm, respectively.

Table I. Kinetic parameters of insulin fibrillation with different ratio concentrations of paclitaxel.

	Lag phase (min)	Lag phase ratio	Growth rate (min^{-1})	Growth rate ratio	Maximum of ThT fluorescence emission	ThT fluorescence emission ratio
Insulin	259.97	1	0.039	1	913.13	1
Paclitaxel						
0.5 μM	303.82	1.16	0.072	1.86	899.10	0.98
5 μM	308.40	1.18	0.047	1.22	456.95	0.50
50 μM	331.92	1.27	0.066	1.69	347.13	0.38

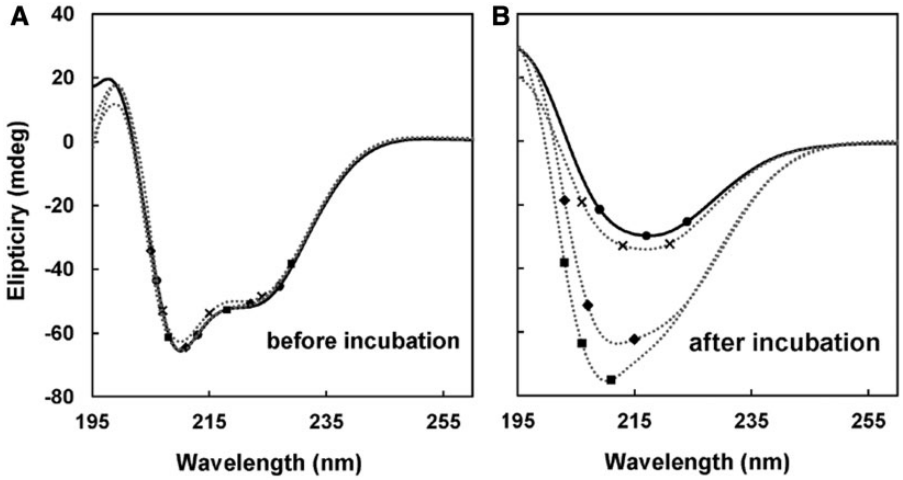

Fig. 2 Secondary structure of insulin was stabilized by paclitaxel. Far-UV-CD spectra of insulin secondary structure: (**A**) before and (**B**) after incubation in the presence of various concentration of paclitaxel: 0 (filled circle), 0.5 (times), 5 (filled diamond) and 50 (filled square) μM.

Exothermic and spontaneous interactions between insulin and paclitaxel

The results of ITC experiment showed that the heat exchange in the interactions of paclitaxel with insulin was exothermic (Fig. 4). Best fitting was carried out in one set of site model, and thermodynamic parameters were obtained for these interactions. As shown in Table II, the number of binding sites for insulin was 1.32, the binding constant for insulin–paclitaxel interaction was $3.06 \times 10^4\,M^{-1}$, and the heat change was acquired as $-1.13 \times 10^5\,cal\,M^{-1}$. The entropy change for insulin interaction was also obtained as $-357\,cal\,M^{-1}\,K^{-1}$. Thus, the extent of Gibbs free energy was calculated as $-6.2 \times 10^3\,cal\,M^{-1}$. As these parameters show, insulin–paclitaxel interaction is enthalpy driven because the negative entropy is thermodynamically unfavourable.

Diminution of salt bridges and dipole moment in insulin dimer

To investigate the possible interaction of paclitaxel with insulin in monomer or aggregate form, we use docking approaches. An ensemble of possible binding sites in an insulin dimer molecule was generated by using HEX. Same calculation was performed to find the possible effects of paclitaxel on insulin dimer formation as a model to investigate the effects of paclitaxel on insulin aggregation. The possible salt bridges that may appear in insulin dimer in the absence or presence of paclitaxel are presented in Fig. 5A and B, respectively. Paclitaxel disrupts some type of possible salt bridges between monomers of insulin. The possible types of salt bridges are scarce in population of insulin dimmers in the presence of paclitaxel. To have an estimate of the effect of paclitaxel on polarity of insulin dimer, the distribution of dipole moment values in insulin dimer in the absence or presence of paclitaxel was computed (Fig. 6). The population of small dipole moment value is the specific result of paclitaxel binding to dimer. Lower dipole support rare possibility of electrostatic interactions and prove the possibility of higher non-electrostatic (hydrophobic) interactions between insulin monomers.

Time-dependent investigation of neurite outgrowth in PC12 cells incubated with insulin fibrils with or without paclitaxel

Cell growth was determined as the following criteria: cell body area, average neurite length and average neurite width. Fig. 7B shows that incubation with insulin fibrils increased cell body area. We measured about 1.8-fold enlargement in insulin-treated groups without paclitaxel at 12 h compared to control. In addition, insulin fibrils diminished neurite length (Fig. 7C). Paclitaxel could modulate these changes, which occurred in cells incubated with insulin fibrils without paclitaxel. The administration of paclitaxel (50 μM) increased neurite length to 2.1-fold at 12 h compared to insulin-treated cells at the same time. Average neurite width measurement, as another criterion showed

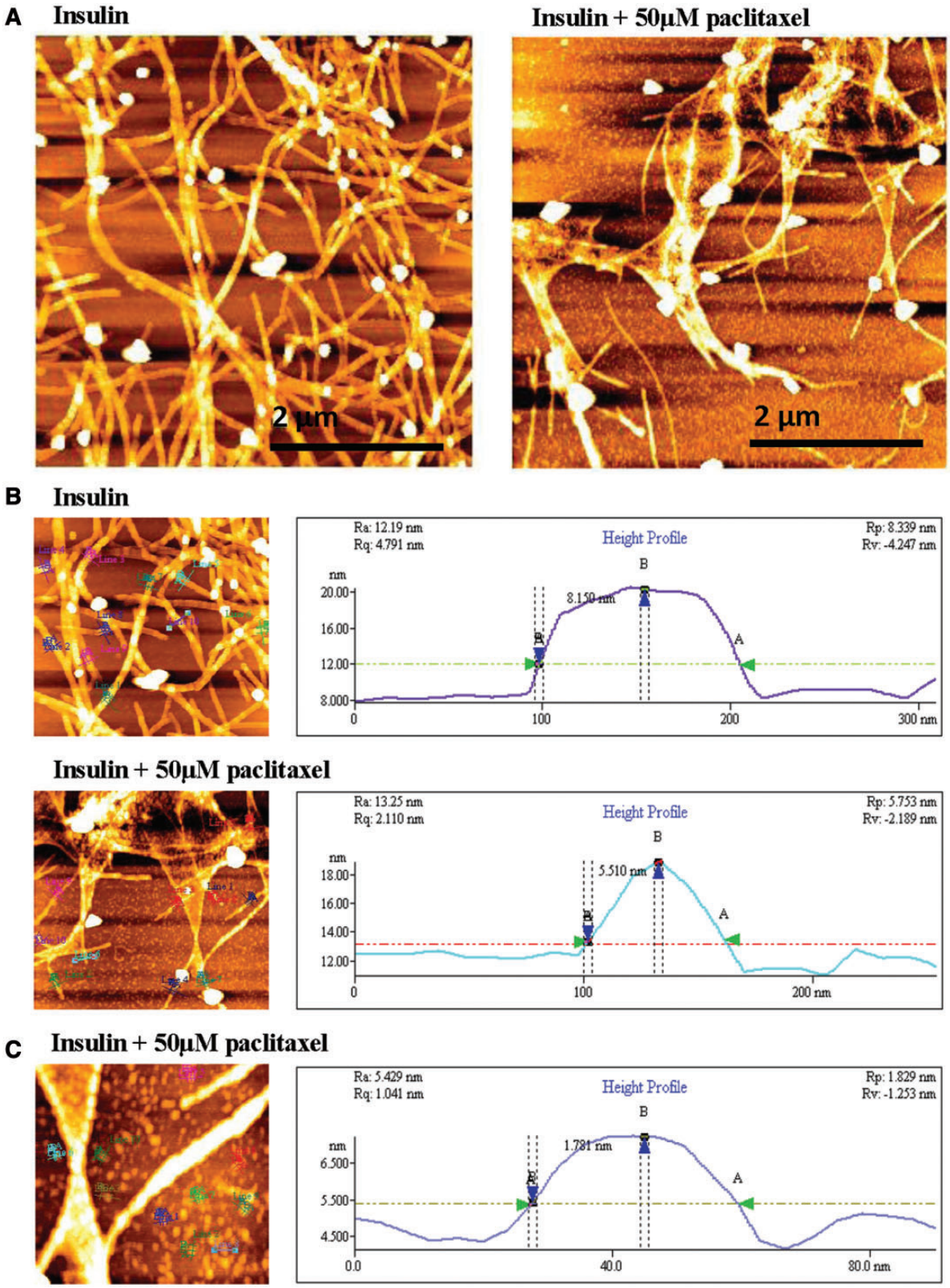

Fig. 3 Paclitaxel inhibited the growth and lateral aggregation of mature insulin amyloid fibrils. (**A**) AFM images visualizing fibril structure of insulin after incubation without or with paclitaxel (50 μM). The scale bars represent 2 μm. (**B**) A 3 μm scale and section profile of fibril images is shown. (**C**) 1 μm scale and section profile of oligomers is shown.

insulin fibrils increased neurite width, while presence of paclitaxel prevented this effect. Neurite width was increased by 4.9-fold in insulin fibril-treated cells without paclitaxel at 12 h compared to control (Fig. 7D). Paclitaxel at 50 μM reduced this increase to 0.3-fold compared with groups with or without paclitaxel at the indicated time (12 h). It is worth mentioning that the time course comparison among cell groups

revealed that the effects of insulin fibrils on PC12 cells was worsen as time passed, especially in those without paclitaxel administration. Fig. 7B, C and D show that the incubation with 50 μM paclitaxel was more effective than lower concentrations of paclitaxel.

Unfavourable effects of insulin fibrils on neurite complexity

Morphological complexity was considered based on the number of primary neurites (>10 μm), per cent of bipolar cells and the ratio of nodes/primary neurites. Fig. 8A shows that the number of primary neurites per cell body was decreased in PC12 cells incubated with insulin fibrils. This reduction was modulated by the administration of different concentrations of paclitaxel. However, the portion of cells with bipolar morphology was increased in those with insulin treatment. Paclitaxel application evaded this morphological condition particularly at 50 μM (Fig. 8B). Computing the ratio of total neurite branching nodes to total number of primary neurites revealed that insulin fibrils could reduce this ratio to 27% of control cells at 12 h (Fig. 8C). Paclitaxel utilization inhibited this reduction to the most extent, i.e. the ratio was increased 3.3-fold in paclitaxel (50 μM)-insulin PC12 cells compared with no paclitaxel incubation (12 h). Thus, the presence of insulin fibrils decreased the morphological complexity of PC12 cells in contrast to those incubated in the presence of paclitaxel.

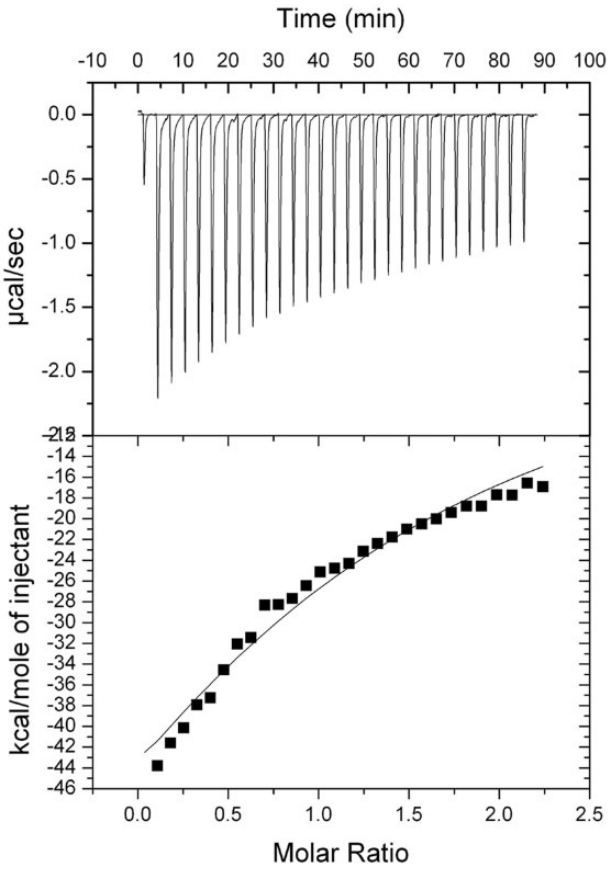

Fig. 4 Exothermic interaction between insulin and paclitaxel. ITC graph of insulin titrated with paclitaxel in 30 injections.

Cell viability analysis and Hoechst staining of cells pretreated with insulin fibrils incubated with or without paclitaxel

To determine the numbers of viable cells MTT assay and Hoechst staining were employed after 12 h of insulin fibrils exposure (Fig. 9A and B). The PC12 cells incubated with insulin fibrils prepared in the presence of paclitaxel exhibited a similar viability as control cells, for the most part, with comparable density and outgrowth of neurites. The MTT assay results indicated that the percentage of cell viability was diminished to 37% in the presence of insulin fibrils after 12 h. However, the cell viability was maintained at an acceptable level of 63% in cells incubated with insulin fibrils prepared in the presence of paclitaxel. As shown in Fig. 9B, Hoechst staining was also brighter in the cells incubated with insulin fibrils compared with cells exposed to insulin fibrils in the presence of paclitaxel. Thus, the presence of paclitaxel prevented the morphological changes occurred in the apoptotic cells indicated by bright blue fluorescence in cells stained with Hoechst.

Discussion

Bovine insulin is structurally similar to human insulin (only differs by three amino acids) which is related to the clinical syndrome injection-localized amyloidosis (*40*, *41*). Fibrillar deposits of insulin have been observed in patients with type II diabetes who have to inject insulin regularly, and as a result of aging (*9*). Previous studies proposed that hydrophobic interactions are key forces in driving insulin fibrillation, and were attributed to the enhanced exposure of buried tryptophans to solvent (*42*). As previously demonstrated, under acidic pH and high temperature conditions insulin monomers become partially folded intermediates (*30*), which provide such hydrophobic regions for subsequent interactions and insulin fibrillation.

The results of Congo red absorbance and ThT fluorescence studies indicated that paclitaxel had an inhibitory effect on formation of beta-sheet and subsequent fibrillation of insulin (Fig. 1). The paclitaxel inhibition was dose dependant, and increased paclitaxel concentrations (up to 50 μM) had a more robust inhibition.

Table II. Thermodynamic parameters of insulin–paclitaxel interactions under acidic condition (pH 1.6).

Complex	N	$K \times 10^4$ (M^{-1})	$\Delta H \times 10^5$ (cal M^{-1})	$T\Delta S \times 10^5$ (cal M^{-1} K^{-1})	$\Delta G \times 10^3$ (cal M^{-1})
Insulin–paclitaxel	1.32 ± 0.379	3.06 ± 1.35	−1.133 ± 0.518	−1.07	−6.2

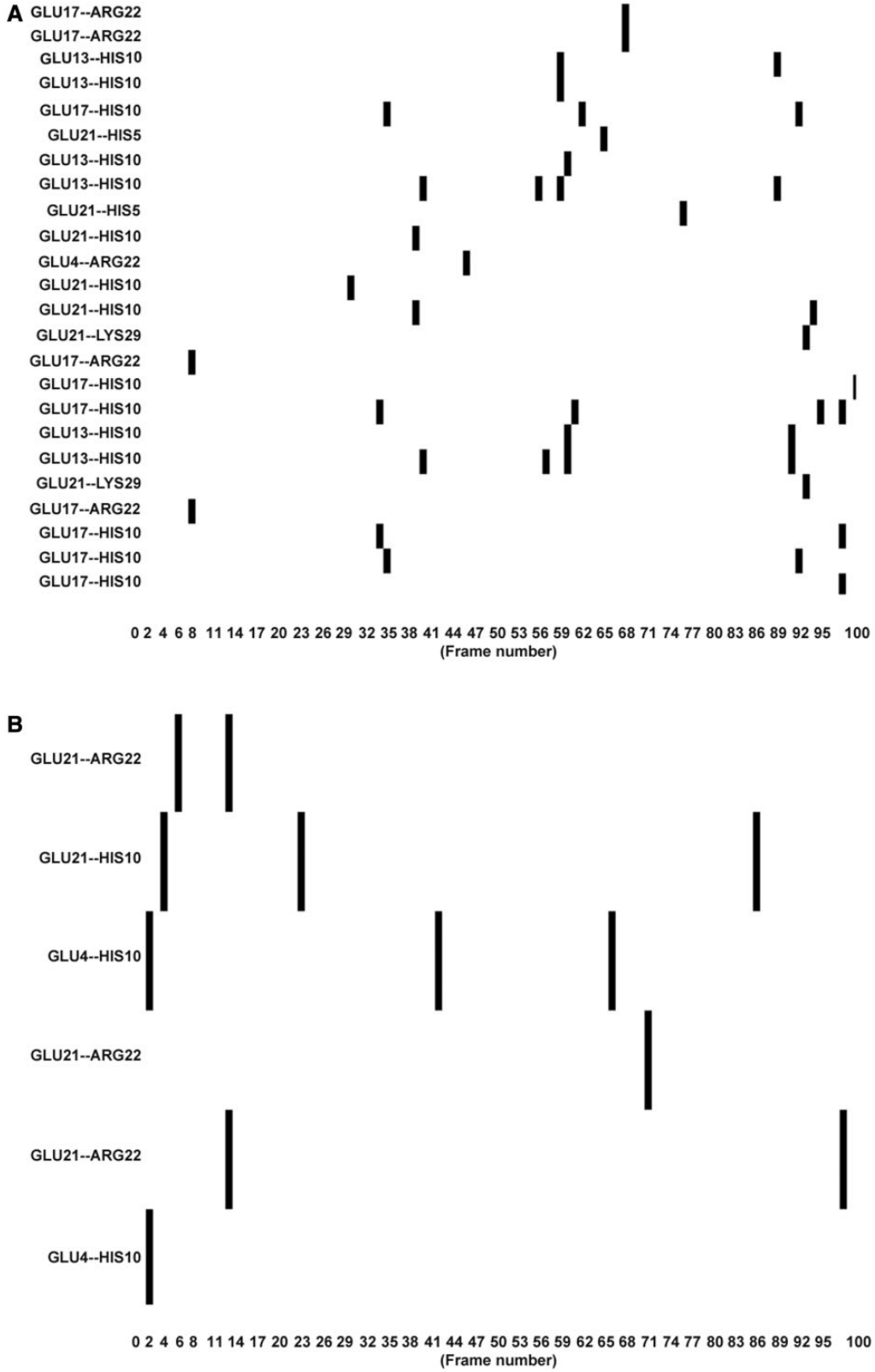

Fig. 5 Paclitaxel diminished salt bridges in insulin dimers. The existence of salt bridges in insulin dimers in the absence (**A**) or presence (**B**) of paclitaxel. The *X*-axis indicates the possible state of the structure (frame), and the salt bridge pairs are indicated in vertical axis.

The AFM images (Fig. 3) confirmed the reduction of insulin fibrillation in the presence of paclitaxel. In addition, these images implied that the paclitaxel hindered the lateral growth of fibril by decreasing fibre diameters. The kinetic studies of insulin fibrillation showed that increased paclitaxel concentration resulted in enhancement of lag phase, which indicated that paclitaxel inhibits the fibrillation process by

hindering the formation of insulin seeding (nuclei). Thus, as a result of lack of critical concentration of insulin seeds fibrillation of insulin was reduced (*17*). Moreover, the elongation study of fibrillation process (Fig. 1C) implied that paclitaxel inhibits the insulin fibrillation in a nucleation-dependent manner and does not influence elongation phase of insulin fibrillation.

In parallel to experimental proofs, computational results indicated that paclitaxel prevents the formation of many salt bridges in insulin dimer (Fig. 5). Thus, paclitaxel may interfere with insulin dimer formation. The distribution of dipole moment in insulin–paclitaxel–insulin structures in comparison with insulin–insulin state indicated that paclitaxel molecules cause the formation of the states with smaller dipole moments (Fig. 6). In performed computation experiments, we found that the insulin dimer state in the presence of paclitaxel was more hydrophobic with lower electrostatic interaction contents. Therefore, in the computation phase of current study we deduced decreasing the polarity of insulin dimer and increasing the hydrophobicity of dimer state by paclitaxel caused an increase in hydrophobic interaction dependent aggregation phase (nucleation). However, it decreased electrostatic-dependent interactions during elongation of aggregation.

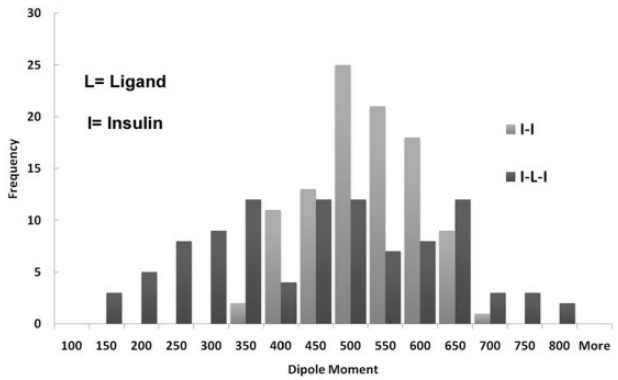

Fig. 6 Paclitaxel caused the formation of insulin dimers by smaller dipole moments. The distribution of molecular dipole moment values of the insulin dimer state in the presence (I-L-I) or absence (I-I) of paclitaxel. The amount of dipole moment in Deby is represented in horizontal axis, and the frequency is indicated in per cent in *Y*-axis.

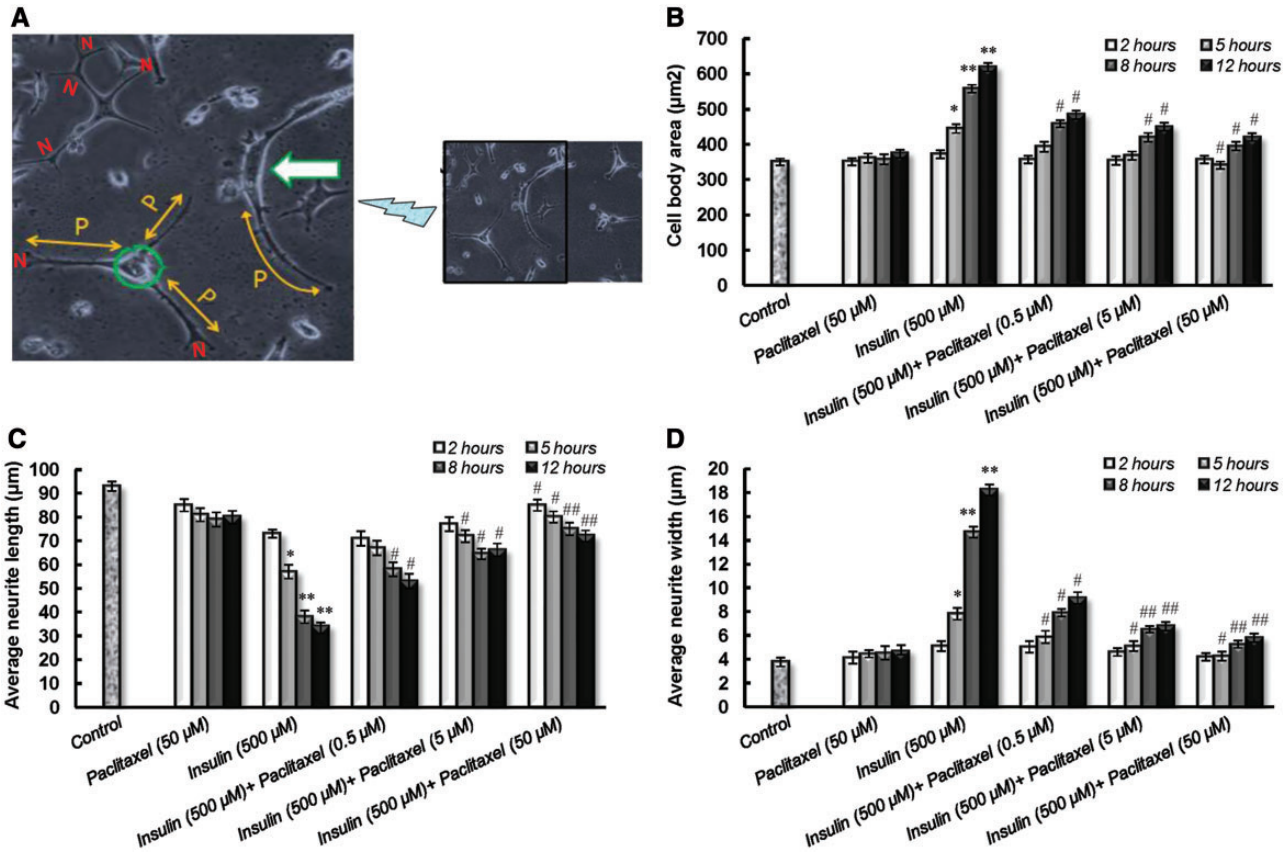

Fig. 7 Evaluation of Neurons by their morphological appearances using phase contrast microscopy. (**A**) The criteria of PC12 differentiation are shown for three neurons from a representative image. The 'P' on left image indicates the primary neuritis of a neuron. The arrows show the length of neurites, the extent of elongation and membrane-enclosed protrusions of the cytoplasm. The circle on left image shows the cell body. The neurite width is not equal in all parts of neurons. Thus, the average neurite width was determined by dividing cell body area to average neurite length. The white arrows point to bipolar cells. The letter 'N' indicates the nodes, the sites at which individual neurites branch or where separate neurites contact each other. These criteria were quantified after different times (2, 5, 8 and 12 h) of incubation with insulin fibrils. (**B**) The effects of paclitaxel (0.5, 5 and 50 μM) on cell body in differentiated PC12 cells incubated with insulin fibrils for different times. (**C**) Average neurite length and (D) Average neurite width PC12 cells incubated with insulin fibrils. Each value represents the mean ± S.E.M. from three independent experiments. Asterisk denotes significantly different from control cells. Statistical significances were achieved when $*p<0.05$ and $**p<0.01$. Hash significantly different from insulin-treated cells at the same times when $^{\#}P<0.05$ and $^{\#\#}P<0.01$.

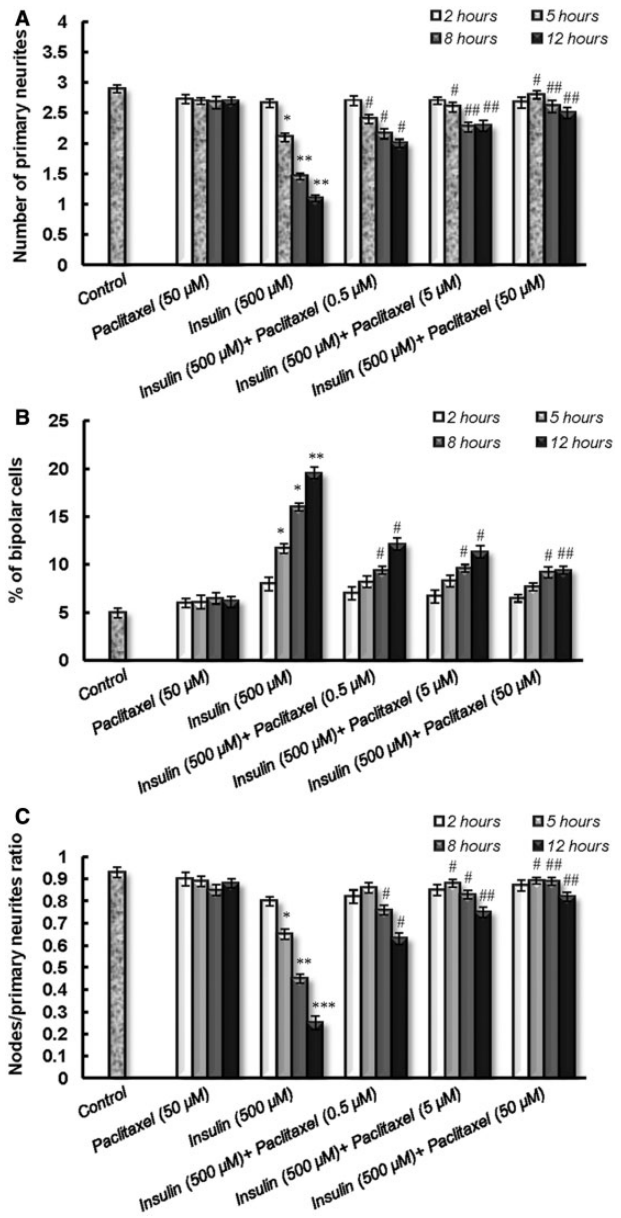

Fig. 8 The effects of insulin fibrils (500 μM) without or with paclitaxel (0.5, 5 and 50 μM) on neurite complexity in differentiated PC12 cells. The indicated criteria were quantified after different times of incubation (2, 5, 8 and 12 h). (**A**) Primary neurites per cell; (**B**) Percent of bipolar cells; and (**C**) The ratio of nodes to primary neurites in differentiated PC12 cells incubated with insulin fibril without or with paclitaxel. Asterisk denotes significantly different from control cells. Statistical significances were achieved when $^{*}p<0.05$ and $^{**}p<0.01$. Hash significantly different from insulin fibril-treated cells without paclitaxel at the same times when $^{\#}P<0.05$ and $^{\#\#}P<0.01$.

Secondary structure of insulin in the presence of paclitaxel did not have any striking changes. These results indicated that the stabilizing effects of paclitaxel on α-helical secondary structure of insulin were responsible for intramolecular forces of insulin monomers to remain undisrupted. Disruption of intramolecular force of insulin monomers was followed by intermolecular interactions, which resulted in its fibrillation. Thus, paclitaxel may hinder insulin fibrillation by stabilizing such intramolecular forces.

In order to explain the interaction of paclitaxel with insulin in acidic pH, thermodynamic studies were conducted using ITC. The results of these studies indicated that this interaction is spontaneous due to negative value of Gibbs free energy (ΔG). In addition, the negative value of both enthalpy change (ΔH) and entropy change (ΔS) indicated a major role for van der Waal's interactions and hydrogen bond formation in paclitaxel–insulin interactions (*43*). Theoretical and practical studies proposed that aromatic interactions, with a striking role for Tyr 16 of the insulin B chain. This residue is considered to be a part of the recognition motif leading to the self-assembly of insulin (*10*) with precise orientation, which is needed in this process, and plays a significant role in protein amyloid self-assembly (*44*, *45*). It has been suggested that polyphenols may suppress amyloid fibril formation by specific aromatic interaction of aromatic residues in the amyloidogenic sequences and their phenol rings (*46*). Paclitaxel has a partially dipole conformation with hydroxyl, carbonyl and carboxyl substituent on one side, and three phenol rings on the other. We presumed that polar side of paclitaxel triggers the formation of paclitaxel–insulin complex by hydrogen bonds, and phenol rings play inhibitory role by pi–pi stacking. Moreover, due to amide and hydroxyl groups which are located near the phenyl rings, paclitaxel aromatic rings are electron poor that limit the possible repulsion between rings and reinforce pi–pi stacking (*47*). Previous studies have shown that a beneficial inhibitor should have either recognition and inhibition/blocking elements (*10*, *48*). We propose that paclitaxel plays such a remarkable role in interactions with insulin.

In our experiments differentiated PC12 cells were utilized due to their sensitivity to neurotoxic materials and common use as an experimental model for neurotoxicity (*9*, *33*, *49*). Fibrillation of insulin could induce the deposits similar to those of Aβ and τ-induced changes. These alternations could contribute to the etiology of Alzheimer's disease, and are believed to take part in many alterations that occur in neuronal structures (*50*). Our data from each criterion of neurite outgrowth and complexity along with Hoechst staining indicated that insulin fibrillation decreased cell viability. This manifestation was much apparent after longer incubation times (8 and 12 h), when the number of bipolar cells with shortened length of their branches was increased. Paclitaxel as a mitotic inhibitor stabilizes microtubules (*22*), and here appeared to stabilize insulin. The circular dichroism results showed that the established neurons without any significant morphological changes are a result of reduction in beta-sheet formation. In agreement, our data revealed paclitaxel's mediatory role in preventing hallmark manifestations of aberrant neurons. Although the current study presents a detailed analysis of the effects of different concentrations of paclitaxel on neuronal morphology in insulin fibril-treated PC12 cells, the involved intracellular mechanisms were not determined and are subject of future studies.

Our results showed that paclitaxel inhibited fibril formation of insulin as a protein model. Inhibition potency of paclitaxel could attribute to the hindering

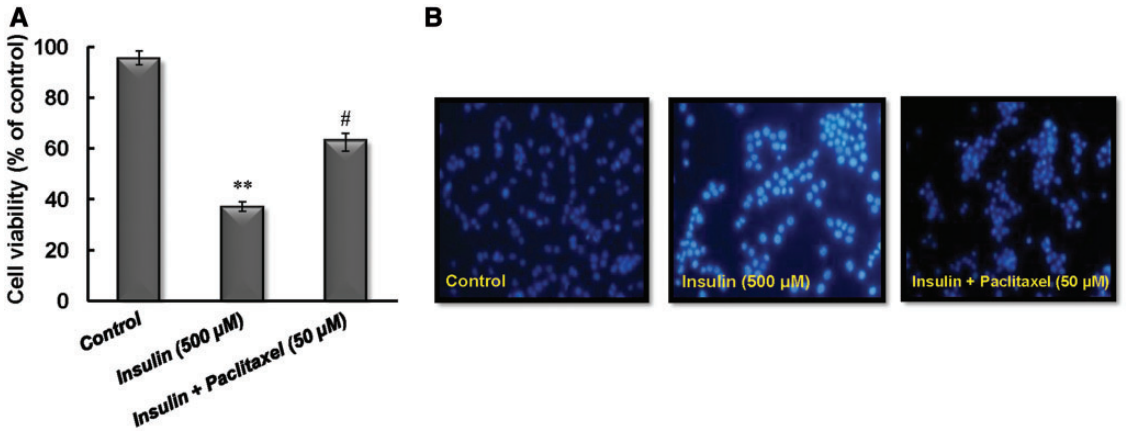

Fig. 9 Determination of cell viability criteria. (A) Cell viability was measured by MTT reduction assay, and cell survival values were expressed as the percentage of control cells after 12 h. (B) Hoechst staining was conducted for evaluation of cell death. Each value represents the mean ± S.E.M. from three independent experiments. Asterisk denotes significantly different from control cells when $*p<0.05$ and $**p<0.01$. Hash significantly different from insulin fibril-treated cells at the same times when $^{\#}P<0.05$.

nucleation of insulin. As indicated in results section, spherical shapes which were observed in AFM images in the presence of paclitaxel imply oligomer formation. We previously showed that oligomeric forms of insulin have neurotoxic effect on PC 12 cells (*33*). Here we showed that the presence of paclitaxel reduced neurotoxicity of insulin fibrils, although the oligomeric forms are observable. These results support the idea that paclitaxel causes formation of 'off-pathway' oligomers which are nontoxic to PC12 cells (*51*). In addition, a low dose of paclitaxel (P/I ≈ 0.1) is sufficient to suppress insulin fibrillation compared to many other inhibitors, which are used at much higher concentrations (*13*, *14*). Finally, the utilization of paclitaxel offers a novel strategy for designing and progression new therapeutic agents in the treatment of diseases related to protein conformational disorders.

Acknowledgements

The support of the University of Tehran, Center of Excellence in Biothermodynamics (CEBiotherm), Iran National Science Foundation (INSF), Iran National Elites Foundation (INEF) and UNESCO Chair on Interdisciplinary Research in Diabetes at University of Tehran is gratefully acknowledged. Special thanks for analysing fluorescence data, in order to kinetic study of fibrillation, by Mohsen Shiea.

Conflict of interest
None declared.

References

1. Herczenik, E. and Gebbink, M.F. (2008) Molecular and cellular aspects of protein misfolding and disease. *FASEB J.* **22**, 2115–2133
2. Dobson, C.M. (2001) The structural basis of protein folding and its links with human disease. *Phil. Trans. R. Soc. B* **356**, 133–145
3. Greenwald, J. and Riek, R. (2010) Biology of amyloid: structure, function, and regulation. *Structure* **18**, 1244–1260
4. Chiti, F. and Dobson, C.M. (2006) Protein misfolding, functional amyloid, and human disease. *Annu. Rev. Biochem.* **75**, 333–366
5. Dobson, C.M. (2003) Protein folding and misfolding. *Nature* **426**, 884–890
6. Ivanova, M.I., Sievers, S.A., Sawaya, M.R., Wall, J.S., and Eisenberg, D. (2009) Molecular basis for insulin fibril assembly. *Proc. Natl Acad. Sci. USA* **106**, 18990–18995
7. Smith, M.I., Sharp, J.S., and Roberts, C.J. (2008) Insulin fibril nucleation: the role of prefibrillar aggregates. *Biophys. J.* **95**, 3400–3406
8. Bucciantini, M., Giannoni, E., Chiti, F., Baroni, F., Formigli, L., Zurdo, J., Taddei, N., Ramponi, G., Dobson, C.M., and Stefani, M. (2002) Inherent toxicity of aggregates implies a common mechanism for protein misfolding diseases. *Nature* **416**, 507–511
9. Wang, S.S.-S., Liu, K.-N., and Han, T.-C. (2010) Amyloid fibrillation and cytotoxicity of insulin are inhibited by the amphiphilic surfactants. *BBA-Mol. Basis. Dis.* **1802**, 519–530
10. Gibson, T.J. and Murphy, R.M. (2006) Inhibition of insulin fibrillogenesis with targeted peptides. *Protein Sci.* **15**, 1133–1141
11. Arora, A., Ha, C., and Park, C.B. (2004) Inhibition of insulin amyloid formation by small stress molecules. *FEBS Lett.* **564**, 121–125
12. Morshedi, D., Rezaei-Ghaleh, N., Ebrahim-Habibi, A., Ahmadian, S., and Nemat-Gorgani, M. (2007) Inhibition of amyloid fibrillation of lysozyme by indole derivatives–possible mechanism of action. *FEBS J.* **274**, 6415–6425
13. Skaat, H., Belfort, G., and Margel, S. (2009) Synthesis and characterization of fluorinated magnetic core–shell nanoparticles for inhibition of insulin amyloid fibril formation. *Nanotechnology* **20**, 225106
14. Levy, M., Porat, Y., Bacharach, E., Shalev, D.E., and Gazit, E. (2008) Phenolsulfonphthalein, but not phenolphthalein, inhibits amyloid fibril formation: implications for the modulation of amyloid self-assembly. *Biochemistry* **47**, 5896–5904
15. Hong, Y., Meng, L., Chen, S., Leung, C.W.T., Da, L.-T., Faisal, M., Silva, D.-A., Liu, J., Lam, J.W.Y., and Huang, X. (2012) Monitoring and inhibition of insulin

fibrillation by a small organic fluorogen with aggregation-induced emission characteristics. *J. Am. Chem. Soc.* **134**, 1680–1689
16. Porat, Y., Abramowitz, A., and Gazit, E. (2006) Inhibition of amyloid fibril formation by polyphenols: structural similarity and aromatic interactions as a common inhibition mechanism. *Chem. Biol. Drug Des.* **67**, 27–37
17. Oliveira, L.M., Lages, A., Gomes, R.A., Neves, H., Família, C., Coelho, A.V., and Quintas, A. (2011) Insulin glycation by methylglyoxal results in native-like aggregation and inhibition of fibril formation. *BMC Biochem.* **12**, 41
18. Lim, G.P., Chu, T., Yang, F., Beech, W., Frautschy, S.A., and Cole, G.M. (2001) The curry spice curcumin reduces oxidative damage and amyloid pathology in an Alzheimer transgenic mouse. *J. Neurosci.* **21**, 8370–8377
19. Schiff, P.B., Fant, J., and Horwitz, S.B. (1979) Promotion of microtubule assembly in vitro by taxol. *Nature* **277**, 665–667
20. Wang, T.H., Wang, H.S., and Soong, Y.K. (2000) Paclitaxel-induced cell death. *Cancer* **88**, 2619–2628
21. Jordan, M.A. and Wilson, L. (2004) Microtubules as a target for anticancer drugs. *Nat. Rev. Cancer.* **4**, 253–265
22. Wani, M.C., Taylor, H.L., Wall, M.E., Coggon, P., and McPhail, A.T. (1971) Plant antitumor agents. VI. The isolation and structure of taxol, a novel antileukemic and antitumor agent from Taxus brevifolia. *J. Am. Chem. Soc.* **93**, 2325–2327
23. Parness, J. and Horwitz, S.B. (1981) Taxol binds to polymerized tubulin in vitro. *J. Cell. Biol.* **91**, 479–487
24. Diaz, J.F., Menendez, M., and Andreu, J.M. (1993) Thermodynamics of ligand-induced assembly of tubulin. *Biochemistry* **32**, 10067–10077
25. Marupudi, N.I., Han, J.E., Li, K.W., Renard, V.M., Tyler, B.M., and Brem, H. (2007) Paclitaxel: a review of adverse toxicities and novel delivery strategies. *Expert Opin. Drug Saf.* **6**, 609–621
26. Michaelis, M.L., Ansar, S., Chen, Y., Reiff, E.R., Seyb, K.I., Himes, R.H., Audus, K.L., and Georg, G.I. (2005) β-Amyloid-induced neurodegeneration and protection by structurally diverse microtubule-stabilizing agents. *J. Pharm. Exp. Ther.* **312**, 659–668
27. Blundell, T., Cutfield, J.F., Cutfield, S.M., Dodson, E., Dodson, G., Hogkin, D., Mercola, D., and Vijayan, M. (1971) Atomic positions in rhombohedral 2-zinc insulin crystals. *Nature* **231**, 506–511
28. Baker, E.N., Blundell, T.L., Cutfield, J.F., Cutfield, S.M., Dodson, E.J., Dodson, G.G., Hodgkin, D.M., Hubbard, R.E., Isaacs, N.W., Reynolds, C.D., Sakabe, K., Sakabe, N., and Vijayan, N.M (1988) The structure of 2Zn pig insulin crystals at 1.5 A resolution. *Phil. Trans. R. Soc. B* **319**, 369–456
29. Bouchard, M., Zurdo, J., Nettleton, E.J., Dobson, C.M., and Robinson, C.V. (2000) Formation of insulin amyloid fibrils followed by FTIR simultaneously with CD and electron microscopy. *Protein Sci.* **9**, 1960–1967
30. Arora, A., Ha, C., and Park, C.B. (2004) Insulin amyloid fibrillation at above 100 degrees C: new insights into protein folding under extreme temperatures. *Protein Sci.* **13**, 2429–2436
31. Nielsen, L., Frokjaer, S., Carpenter, J.F., and Brange, J. (2001) Studies of the structure of insulin fibrils by Fourier transform infrared (FTIR) spectroscopy and electron microscopy. *J. Pharm. Sci.* **90**, 29–37
32. Ahmad, A., Millett, I.S., Doniach, S., Uversky, V.N., and Fink, A.L. (2004) Stimulation of insulin fibrillation by urea-induced intermediates. *J. Biol. Chem.* **279**, 14999–15013
33. Kachooei, E., Moosavi-Movahedi, A.A., Khodagholi, F., Ramshini, H., Shaerzadeh, F., and Sheibani, N. (2012) Oligomeric forms of insulin amyloid aggregation disrupt outgrowth and complexity of neuron-like pc12 cells. *PLoS One* **7**, e41344
34. Grudzielanek, S., Velkova, A., Shukla, A., Smirnovas, V., Tatarek-Nossol, M., Rehage, H., Kapurniotu, A., and Winter, R. (2007) Cytotoxicity of insulin within its self-assembly and amyloidogenic pathways. *J. Mol. Biol.* **370**, 372–384
35. Skora, L., Becker, S., and Zweckstetter, M. (2010) Molten globule precursor states are conformationally correlated to amyloid fibrils of human β-2-microglobulin. *J. Am. Chem. Soc.* **132**, 9223–9225
36. Dzwolak, W., Loksztejn, A., and Smirnovas, V. (2006) New insights into the self-assembly of insulin amyloid fibrils: an HD exchange FT-IR study. *Biochemistry* **45**, 8143–8151
37. Naiki, H., Higuchi, K., Hosokawa, M., and Takeda, T. (1989) Fluorometric determination of amyloid fibrils in vitro using the fluorescent dye, thioflavine T. *Anal. Biochem.* **177**, 244–249
38. Nielsen, L., Khurana, R., Coats, A., Frokjaer, S., Brange, J., Vyas, S., Uversky, V.N., and Fink, A.L. (2001) Effect of environmental factors on the kinetics of insulin fibril formation: elucidation of the molecular mechanism. *Biochemistry* **40**, 6036–6046
39. Eisert, R., Felau, L., and Brown, L.R. (2006) Methods for enhancing the accuracy and reproducibility of Congo red and thioflavin T assays. *Anal. Biochem.* **353**, 144–146
40. Dische, F., Wernstedt, C., Westermark, G., Westermark, P., Pepys, M., Rennie, J., Gilbey, S., and Watkins, P. (1988) Insulin as an amyloid-fibril protein at sites of repeated insulin injections in a diabetic patient. *Diabetologia* **31**, 158–161
41. Manno, M., Craparo, E.F., Podestà, A., Bulone, D., Carrotta, R., Martorana, V., Tiana, G., and San Biagio, P.L. (2007) Kinetics of different processes in human insulin amyloid formation. *J. Mol. Biol.* **366**, 258–274
42. Sluzky, V., Tamada, J.A., Klibanov, A.M., and Langer, R. (1991) Kinetics of insulin aggregation in aqueous solutions upon agitation in the presence of hydrophobic surfaces. *Proc. Natl Acad. Sci. USA* **88**, 9377–9381
43. Ross, P.D. and Subramanian, S. (1981) Thermodynamics of protein association reactions: forces contributing to stability. *Biochemistry* **20**, 3096–3102
44. Jack, E., Newsome, M., Stockley, P.G., Radford, S.E., and Middleton, D.A. (2006) The organization of aromatic side groups in an amyloid fibril probed by solid-state 2H and 19F NMR spectroscopy. *J. Am. Chem. Soc.* **128**, 8098–8099
45. Tartaglia, G.G., Cavalli, A., Pellarin, R., and Caflisch, A. (2004) The role of aromaticity, exposed surface, and dipole moment in determining protein aggregation rates. *Protein Sci.* **13**, 1939–1941
46. Porat, Y., Mazor, Y., Efrat, S., and Gazit, E. (2004) Inhibition of islet amyloid polypeptide fibril formation: a potential role for heteroaromatic interactions. *Biochemistry* **43**, 14454–14462

47. Levy-Sakin, M., Shreberk, M., Daniel, Y., and Gazit, E. (2009) Targeting insulin amyloid assembly by small aromatic molecules: toward rational design of aggregation inhibitors. *Islets* **1**, 210–215
48. Frydman-Marom, A., Rechter, M., Shefler, I., Bram, Y., Shalev, D.E., and Gazit, E. (2009) Cognitive-performance recovery of Alzheimer's disease model mice by modulation of early soluble amyloidal assemblies. *Angew. Chem. Int. Ed.* **121**, 2015–2020
49. Zako, T., Sakono, M., Hashimoto, N., Ihara, M., and Maeda, M. (2009) Bovine insulin filaments induced by reducing disulfide bonds show a different morphology, secondary structure, and cell toxicity from intact insulin amyloid fibrils. *Biophys. J.* **96**, 3331–3340
50. Marwarha, G., Dasari, B., Prasanthi, J.R., Schommer, J., and Ghribi, O. (2010) Leptin reduces the accumulation of Aβ and phosphorylated τ induced by 27-hydroxycholesterol in rabbit organotypic slices. *J. Alzheimers Dis.* **19**, 1007–1019
51. Ehrnhoefer, D.E., Bieschke, J., Boeddrich, A., Herbst, M., Masino, L., Lurz, R., Engemann, S., Pastore, A., and Wanker, E.E. (2008) EGCG redirects amyloidogenic polypeptides into unstructured, off-pathway oligomers. *Nat. Struct. Mol. Biol.* **15**, 558–566